THE JOURNAL OF BIOLOGICAL CHEMISTRY VOL. 281, NO. 48, pp. 37175–37182, December 1, 2006
Printed in the U.S.A.

Crystal Structures of *Aedes aegypti* Alanine Glyoxylate Aminotransferase*

Received for publication, July 24, 2006, and in revised form, September 6, 2006 Published, JBC Papers in Press, September 21, 2006, DOI 10.1074/jbc.M607032200

Qian Han[‡], Howard Robinson[§], Yi Gui Gao[¶], Nancy Vogelaar[‖], Scott R. Wilson[¶], Menico Rizzi[**], and Jianyong Li[‡1]

*From the [‡]Department of Biochemistry, Virginia Tech, Blacksburg, Virginia 24061, the [§]Biology Department, Brookhaven National Laboratory, Upton, New York 11973, the [¶]School of Chemical Sciences, University of Illinois, Urbana, Illinois 61801, the [‖]Department of Biology, Virginia Tech, Blacksburg, Virginia 24061, and the **Structural Biology Unit, University of Piemonte Orientale Novara, 28100 Novara, Italy*

Mosquitoes are unique in having evolved two alanine glyoxylate aminotransferases (AGTs). One is 3-hydroxykynurenine transaminase (HKT), which is primarily responsible for catalyzing the transamination of 3-hydroxykynurenine (3-HK) to xanthurenic acid (XA). Interestingly, XA is used by malaria parasites as a chemical trigger for their development within the mosquito. This 3-HK to XA conversion is considered the major mechanism mosquitoes use to detoxify the chemically reactive and potentially toxic 3-HK. The other AGT is a typical dipteran insect AGT and is specific for converting glyoxylic acid to glycine. Here we report the 1.75 Å high-resolution three-dimensional crystal structure of AGT from the mosquito *Aedes aegypti* (AeAGT) and structures of its complexes with reactants glyoxylic acid and alanine at 1.75 and 2.1 Å resolution, respectively. This is the first time that the three-dimensional crystal structures of an AGT with its amino acceptor, glyoxylic acid, and amino donor, alanine, have been determined. The protein is dimeric and adopts the type I-fold of pyridoxal 5-phosphate (PLP)-dependent aminotransferases. The PLP co-factor is covalently bound to the active site in the crystal structure, and its binding site is similar to those of other AGTs. The comparison of the AeAGT-glyoxylic acid structure with other AGT structures revealed that these glyoxylic acid binding residues are conserved in most AGTs. Comparison of the AeAGT-alanine structure with that of the *Anopheles* HKT-inhibitor complex suggests that a Ser-Asn-Phe motif in the latter may be responsible for the substrate specificity of HKT enzymes for 3-HK.

Mosquitoes transmit malaria, which is considered the most prevalent life-threatening disease in the world (1). In mosquitoes, transamination of 3-hydroxykynurenine (3-HK)[2] to xanthurenic acid (XA) is the major branch pathway of tryptophan metabolism (2, 3). XA has been identified as a natural chemical signal produced by mosquitoes, which induces exflagellation of malaria parasites in the midgut (4, 5). Recently, we reported that mosquitoes have evolved two alanine glyoxylate aminotransferases (6). One is the previously cloned *Aedes aegypti* 3-HK transaminase (AeHKT) (3), homologous to human AGT (hAGT), which primarily catalyzes the transamination of 3-HK to XA in mosquitoes. The other is a typical dipteran insect AGT, which primarily catalyzes the conversion of glyoxylic acid to glycine (6). A BLAST search of the genomes of other available model species (including cyanobacteria, archaea, yeast, plants, fruit fly, honeybee, frog, fish, rat, mouse, and human) revealed only one AGT in their genomes, which makes possessing two AGTs a unique property of mosquitoes. Based on both phylogenetic analysis and biochemical characterization, AeAGT is closely related to *Drosophila* AGT (DrAGT) and AeHKT is closely related to hAGT (6, 7).

The different roles of these two aminotransferases in the mosquito may be better understood by examining their substrate specificities and temporal expression patterns in the context of the mosquito life cycle, discussed in more detail previously (6). Mosquito larvae eat protein-rich food, and a considerable portion of the tryptophan obtained from these food supplies is oxidized to 3-HK (2). In humans and other mammals, kynurenine aminotransferase I and II catalyze the transamination of kynurenine to kynurenic acid and 3-HK to XA (8–10). *Ae. aegypti* kynurenine aminotransferase shows high activity toward kynurenine but no activity toward 3-HK (10–12). In contrast, conversion of 3-HK to XA is catalyzed mainly by AeHKT in *Ae. aegypti* mosquitoes. Because mosquitoes cannot dispose of 3-HK through hydrolysis and subsequent oxidations like mammals, the transamination of the chemically reactive 3-HK to the relatively chemically stable XA by HKT is considered the mechanism by which mosquitoes prevent 3-HK from overaccumulating (7). Such an explanation remains a valid argument for the functional evolution of the mosquito AGTs. Interestingly, 3-HK is also the initial precursor for the production of ommochromes that are major eye pigments in mosquitoes. Compound eye development and eye pigmentation occur mainly during the pupal and early adult stages.

* This work was supported by Grant RO1 AI44399 from the National Institutes of Health and a grant from Regione Piemonte, Project "Ricerca scientifica applicata 2003." The costs of publication of this article were defrayed in part by the payment of page charges. This article must therefore be hereby marked "*advertisement*" in accordance with 18 U.S.C. Section 1734 solely to indicate this fact.

The atomic coordinates and structure factors (code 2huf, 2hui, and 2huu) have been deposited in the Protein Data Bank, Research Collaboratory for Structural Bioinformatics, Rutgers University, New Brunswick, NJ (http://www.rcsb.org/).

[1] To whom correspondence should be addressed: Dept. of Biochemistry, Virginia Tech, Blacksburg, VA 24061. Tel.: 540-231-1182; Fax: 540-231-9070; E-mail: lij@vt.edu.

[2] The abbreviations used are: 3-HK, 3-hydroxykynurenine; AeAGT, *Ae. aegypti* alanine glyoxylate aminotransferase; AeHKT, *Ae. aegypti* HKT; AGT, alanine glyoxylate aminotransferase; AnHKT, *Anopheles* HKT; DrAGT, *Drosophila* AGT; hAGT, human AGT; HKT, 3-HK transaminase; LLP, lysine-pyridoxal 5-phosphate; PLP, pyridoxal 5-phosphate; XA, xanthurenic acid.

TABLE 1

Data collection and refinement statistics

BNL, Brookhaven National Laboratory; r.m.s., root mean square.

	Crystal data		
	AeAGT	AeAGT-Glyoxylic acid	AeAGT-Alanine
Space group		*R*3	
Unit cell (Å)			
$a = b$	137.0	137.1	137.1
c	120.3	120.4	120.3
Data collection			
X-ray source		BNL-X25	
Wavelength (Å)		0.9795	
Resolution (Å)[a]	1.75 (1.81-1.75)	1.75 (1.81-1.75)	2.1 (2.18-2.1)
Total number of reflections	934,979	847,382	56,301
No. of unique reflections	84,824	85,152	49,270
R-merge[a]	0.081 (0.484)	0.103 (0.569)	0.093 (0.483)
Redundancy[a]	11 (8.0)	10.3 (3.3)	11.4 (11.2)
Completeness (%)[a]	100 (100)	97 (72)	100 (100)
Refinement statistics			
R-work (%)	17.2	17.5	15
R-free (%)	20.3	20.6	19.5
No. of reflections (*R*-free)	4,233	4,106	2,493
r.m.s. bond lengths (Å)	0.013	0.014	0.018
r.m.s. bond angles (°)	1.635	1.695	1.895
No. of protein residues		2 × 385	
No. of LLP molecules	2	2	2
No. of butanol molecules	2		1
No. of glyoxylic acid molecules		2	
No. of alanine molecules			1
No. of solvent molecules (water)	521	579	637
Average B overall (Å^2)	18.6	15.7	25.7
Ramachandran analysis (% of residues)			
Most favored	93.7	93.1	94.0
Additional allowed	6.1	6.7	6.0
Generously allowed	0.2	0.2	0.0

[a] The values in parentheses are for the highest resolution shell.

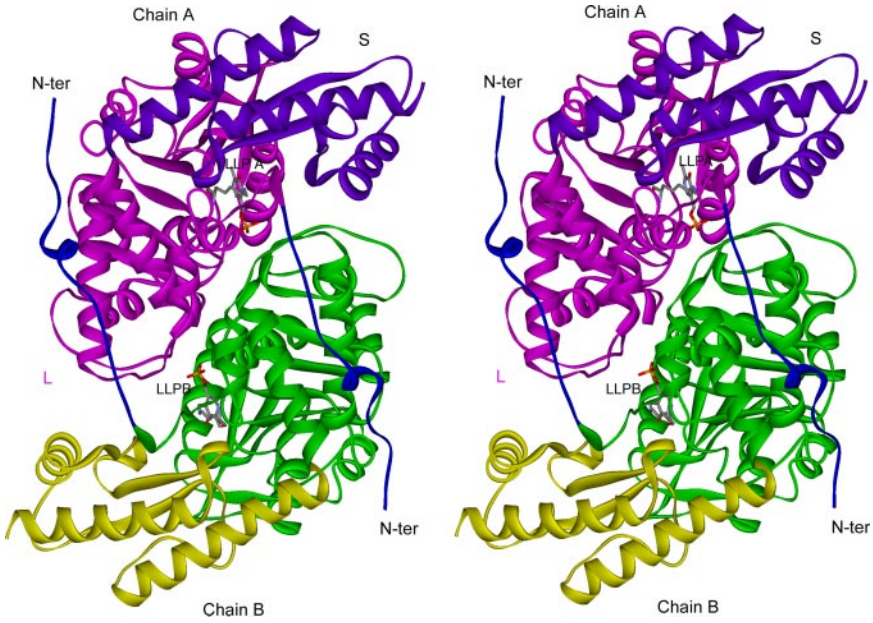

FIGURE 1. **Stereo schematic representation of the structure of the AeAGT dimer.** The large domains (*L*) in both subunits are colored in *pink* and *green*, respectively; the small domains (*S*) in both units are colored in *purple* and *orange*, respectively. Both arms (*N-ter*) are colored in *blue*. The two active sites at the interface of the subunits are shown with the LLP (lysine-pyridoxal 5-phosphate) in element-colored *sticks* (*light gray*, carbon; *blue*, nitrogen; *red*, oxygen; *orange*, phosphorus).

Coincidently, HKT activity is diminished in pupae and adults correlating with the accumulation of high levels of 3-HK in the compound eyes (13). The down-regulation of AeHKT is likely a tactic to allow 3-HK to be transported and used for eye pigmentation. Although it seems clear that detoxification of 3-HK is a major function of AeHKT in mosquito larvae, the enzyme exhibits high AGT activity and likely plays a critical role in metabolizing glycolate-derived glyoxylate as well, especially in adults, because males eat the part of plants that is normally glycolate-rich. Consequently, the interruption of AeHKT expression during the adult stages would affect the metabolism of glyoxylic acid. Therefore, a highly substrate-specific (*i.e.* highly active with regard to the glyoxylic acid to glycine pathway but without detectable HKT activity) and stage-specific AeAGT has evolved in mosquitoes.

Biochemical characterization shows that AeAGT is highly specific for catalyzing glyoxylic acid to glycine processing. AeHKT, on the other hand, primarily catalyzes the transamination of 3-HK to XA but also exhibits the same activities as AeAGT. To understand the structural basis underlying the stringent substrate specificity of AeAGT as compared with that of AeHKT, it is essential to determine the three-dimensional structure of AeAGT. In this

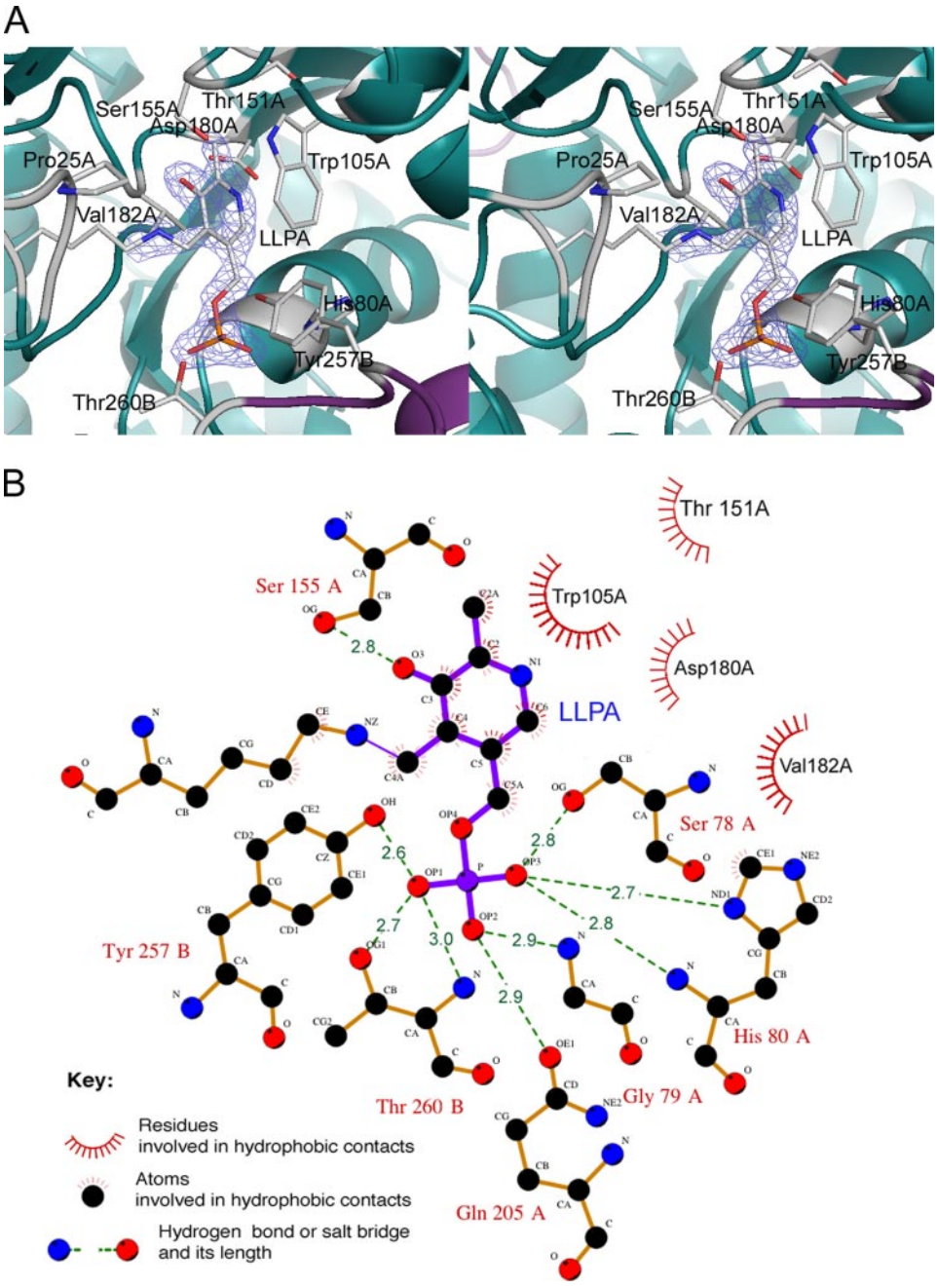

FIGURE 2. **The AeAGT active site.** *A*, stereo view of the active site in the AeAGT structure. The protein portions building up the active site and contributed to by the two subunits of the functional homodimer are shown in a schematic representation and are colored in *deep teal* (subunit A) and *violet* (subunit B). The PLP cofactor and the protein residues within a 4-Å distance of PLP are shown. Only the $2F_o - F_c$ electron density map covering the LLPA is shown contoured at the 1.8 sigma level. This panel was generated using Pymol. *B*, schematic view of the AeAGT active site. The key interactions involving PLP binding are indicated together with the distances for hydrogen bonds or salt bridges observed in the AeAGT structure. This panel was generated using Ligplot.

study, we determined the native three-dimensional crystal structure of AeAGT as well as the structures with its specific substrates, alanine and glyoxylic acid, respectively. This is the first time the crystal structures of the enzyme-substrate complexes for AGTs have been reported. We have also compared AeAGT complex structures with the available AGT structures and discussed the possible residues involved in substrate specificity. The results from this study, in conjunction with the results of previous studies dealing with the molecular and biochemical characterization of AeHKT (3, 7), AeAGT (6), and the three- dimensional structural study of *Anopheles* HKT (AnHKT) (14), provide an interesting example of protein functional adaptation and evolution, in this case to meet certain physiological requirements during development.

MATERIALS AND METHODS

Overexpression and Purification of AeAGT Recombinant Protein—Full-length AeAGT was overexpressed in a baculovirus/insect cell protein expression system (Invitrogen). The recombinant AeAGT was purified as described previously (6). The molecular weight and purity of the proteins were assessed by SDS-PAGE analysis. Protein concentrations were determined using a Bio-Rad protein assay kit using bovine serum albumin as a standard.

AeAGT Crystallization and Substrate Soaking—Initial crystallization screening was performed using Hampton Research Crystal Screens (Hampton Research, Laguna Niguel, CA) using the hanging drop vapor diffusion method. The volume of reservoir solution was 500 μl, and the drop volume was 2 μl, containing 1 μl of protein sample and 1 μl of reservoir solution. Quality AeAGT crystals were obtained in a solution containing 5 mg ml^{-1} protein, 12% polyethylene glycol 8000, 0.13 M magnesium acetate, 4% butanol, and 0.1 M cacodylic acid at pH 6.5. Single crystals suitable for x-ray analysis appeared within 1 to 2 weeks at 4 °C. Alanine-enzyme and glyoxylic acid-enzyme complexes were obtained by soaking the crystals in 2.5 mM alanine and 1 mM glyoxylic acid, respectively, in the crystallization buffer for 1 week.

Data Collection and Processing—Individual AeAGT crystals were cryogenized using 25% glycerol in crystallization buffer as a cryoprotectant solution. Diffraction data from AeAGT crystals were collected at the Brookhaven National Synchrotron Light Source, Beamline X25 (λ = 0.9795 Å). Data collection was done using an ADSC Q315 charge-coupled device detector. All data were indexed and integrated using HKL software (15), and scaling and merging of diffraction data were performed using the program SCALEPACK (16). The parameters of the crystals and data collection are listed in Table 1.

Structure Determination—The structure of AeAGT was determined by the molecular replacement method. The initial search model was built with the homology module in Insight II (Accelrys) using hAGT (Protein Data Bank code 1h0c) as the template structure (17). The program Molrep (18) in the CCP4 suite was employed to calculate both the cross-rotation and translation of the homology model. The initial model was subjected to iterative cycles of crystallographic refinement with Refmac 5.2 (19) and graphic sessions for model building using the program O (20). Solvent molecules were automatically added and refined with ARP/wARP (21) together with Refmac 5.2. For the AeAGT structure, a careful inspection of the electron density in the enzyme active site was performed when the *R*-factor dropped to a value of 0.20 at 1.75 Å. This revealed an electron density compatible with one butanol molecule, which was subsequently manually modeled based on both the $2F_o - F_c$ and $F_o - F_c$ electron density maps. The AeAGT-alanine and AeAGT-glyoxylic acid complex structures were refined by using the final coordinates of the AeAGT native structure as the starting model from which all solvent and butanol molecules were removed. The substrate molecules were modeled only when the *R*-factor dropped to a value of 0.2 at full resolution for the AeAGT-alanine structure and a value of 0.2 at 1.75 Å resolution for the AeAGT-glyoxylic acid structure.

Structure Analysis—Superposition of structures was done using Lsqkab (22) in the CCP4 suite. Protein and substrate interaction was analyzed using Ligplot (23). The figures were generated using Pymol (24) and Ligplot (23).

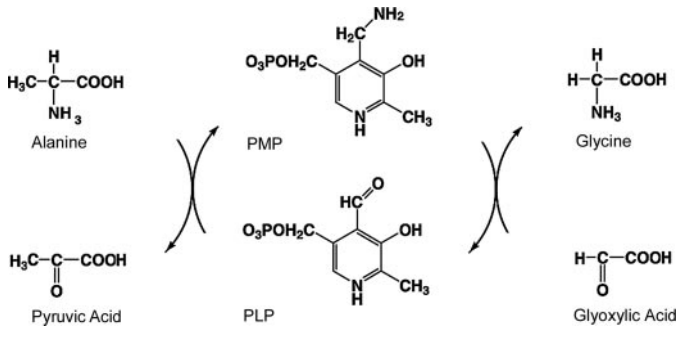

SCHEME 1

RESULTS AND DISCUSSION

Overall Structure—The structure of AeAGT was determined by molecular replacement and refined to 1.75 Å resolution. The final model contains 385 residues, yielding a crystallographic *R*-value of 17.3% and an R_{free} value of 20.3% with ideal geometry (Table 1). There are two molecules in an asymmetric unit that form the homodimer. The residues of the two subunits in AeAGT are numbered 1A to 385A for chain A and 1B to 385B for chain B. The refinement results are summarized in Table 1.

All residues are in favorable regions of the Ramachandran plot as defined with PROCHECK (25). The last eight residues (386–393) were not defined in the $2F_o - F_c$ electron density map and are absent from the final model. The protein architecture revealed by AeAGT consists of the prototypical fold of aminotransferase subgroup I (26, 27), characterized by an N-terminal arm, which consists of a random coiled stretch made of residues 1–18, a small C-terminal domain (residues 280–385), and a large N-terminal domain (residues 19–279) (Fig. 1), which is similar to the reported AGT structures from other species (14, 17, 28, 29). As

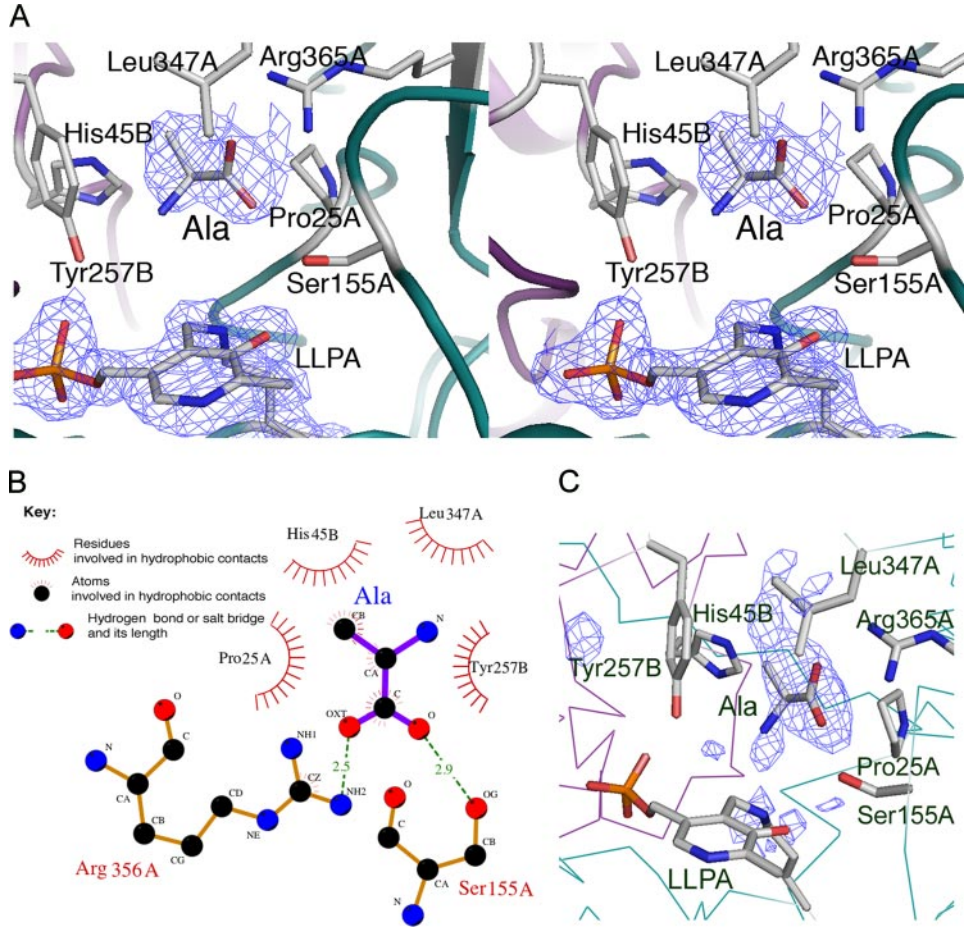

FIGURE 3. **Alanine binding site.** *A*, stereo view of the alanine binding site in the AeAGT-alanine structure. The protein portions building up the binding site and contributed to by the two subunits of the functional homodimer, shown in a schematic representation, are colored in *deep teal* (subunit A) and *violet* (subunit B), respectively. The alanine substrate (Ala) and the protein residues within 4 Å distance of the alanine substrate are shown. The $2F_o - F_c$ electron density map covering the alanine and LLPA is shown contoured at the 0.7 sigma level. This panel was generated using Pymol. *B*, schematic view of the alanine binding site. The key interactions involving alanine binding are indicated together with the distances for hydrogen bonds or salt bridges observed in the AeAGT-alanine structure. This panel was generated using Ligplot. *C*, the omit map calculated without the alanine substrate is shown as an $F_o - F_c$ electron density map contoured at the 2 sigma level. Subunits A and B are colored in *deep teal* and *violet*, respectively.

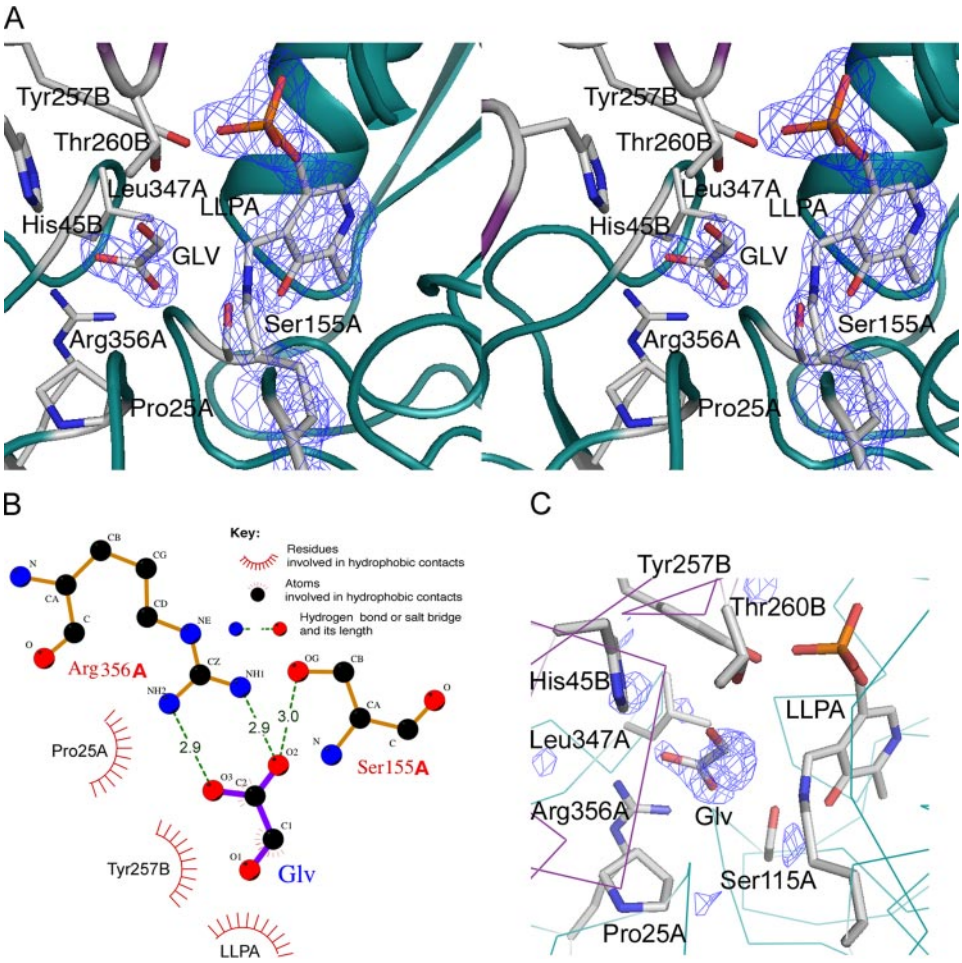

FIGURE 4. **Glyoxylic acid binding site.** *A*, stereo view of the glyoxylic acid binding site in the AeAGT-glyoxylic acid structure. The protein portions building up the binding site and contributed to by the two subunits of the functional homodimer are shown in a schematic representation and colored in *deep teal* (subunit A) and *violet* (subunit B). The glyoxylic acid substrate (*GLV*) and the protein residues within 4 Å distance of glyoxylic acid are shown. The $2F_o - F_c$ electron density map covering the glyoxylic acid and LLPA is shown contoured at the 1.8 sigma level. This panel was generated using Pymol. *B*, schematic view of the glyoxylic acid binding site. The key interactions involving glyoxylic acid binding are indicated together with the distances for hydrogen bonds or salt bridges observed in the AeAGT-glyoxylic acid structure. This panel was generated using Ligplot. *C*, the omit map calculated without the glyoxylic acid substrate is shown as an $F_o - F_c$ electron density map contoured at the 2 sigma level. Subunits A and B are colored in *deep teal* and *violet*, respectively.

observed in other subgroup I aminotransferases, the functional unit of AeAGT consists of a homodimer.

Active Site of AeAGT—Residual electron density clearly revealed the presence of covalently bound pyridoxal 5-phosphate (PLP) in the cleft situated at the interface of the subunits in the biological dimer (Figs. 1 and 2*A*). This cleft also corresponds to the cofactor binding sites in the related enzymes and therefore defines the active site of AeAGT. The C4A atom of PLP is covalently attached to the NZ of Lys^{206A} through the formation of an internal Schiff base, the internal aldimine giving rise to residue LLPA, represented as *sticks* in Fig. 2*A*. The PLP-pyridoxal ring is stacked between residues Trp^{105A} and Val^{182A} by hydrophobic interactions, and the C2A atom of PLP exhibits hydrophobic interaction with the Thr^{151A} side chain. The side chains of Ser^{155A} and Asp^{180A} are hydrogen-bonded to O-3 and N-1 of the pyridoxal, respectively. The phosphate moiety of the PLP is anchored by polar interactions with the peptide amide groups of residues Gly^{79A} and His^{80A} as well as by the side chains of Ser^{78A}, His^{80A}, and Gln^{205A}. The binding site of the PLP-phosphate is completed by hydrogen bonds with the side chains of Tyr^{257B} and Tyr^{260B} from the second subunit in the biological dimer (Fig. 2*B*). The N-terminal extension makes a turn around residues Gly^{24A}, Pro^{25A}, and Gly^{26A} exposing the Pro^{25A} carbonyl group toward the active site. This conformation allows for polar interaction with the NZ of Lys^{206A} and could also interact with the amino group from the pyridoxamine intermediate during the enzymatic reaction.

Substrate Recognition and Catalysis—Enzyme activity assays of AeAGT revealed that alanine acts efficiently as an amino group donor substrate during the transamination reaction, yielding pyruvate, and glyoxylic acid acts efficiently as an amino acceptor, yielding glycine (6). The enzyme-catalyzed reaction is shown in Scheme 1.

To identify the structural determinants of AeAGT involved in substrate recognition and binding, we determined the three-dimensional crystal structures of the enzyme in complex with alanine (Fig. 3) and glyoxylic acid (Fig. 4). Inspection of the AeAGT-alanine complex crystal structure reveals that the substrate lies near the internal Schiff base between the PLP cofactor and the NZ of Lys^{206A}. However, PLP is still in its internal aldimine form (Fig. 3). Several residues, structurally conserved throughout the aminotransferases described thus far, define the substrate binding site and contact the alanine molecule. In particular, Arg^{356A} forms a strong salt bridge with the alanine carboxylate group at a distance of 2.5 Å. A hydrogen-bonding network, involving Ser^{155A} and Gly^{345A} backbone oxygen atoms, locks the Arg^{356A} side chain in the optimal conformation for alanine binding. The anchoring of the alanine carboxylic moiety by Arg^{356A} in the AeAGT-alanine complex (Fig. 3) results in the reactive α-amino group being placed into the ideal position (the nitrogen atom is above the PLP C4A reactive center at a distance of 3.7 Å) for attacking the PLP C4A atom and forming the external aldimine. The alanine is also recognized by a number of interactions with protein residues, including Tyr^{257B}, His^{45B}, Pro^{25A}, Ser^{155A}, and Leu^{347A} (Fig. 3). Gly^{26A} is located at the turning point of the loop that dives into and partially plugs the enzyme active site, thus shielding the substrate binding pocket from the bulk solvent. It is interesting that alanine was found only in one subunit of the dimer. Alanine is a primary amino acid substrate for most of AGTs, but its K_m is much higher than glyoxylic acid,

and therefore this might be a reason that the alanine concentration in the soaking solution was not high enough for the amino acid to get into the active site of the enzyme in all of the molecules of the crystal. A similar behavior was observed in the complex of *Paracoccus denitrificans* aromatic amino acid aminotransferase with 3-phenylpropionate (30).

Glyoxylic acid is the most physiologically relevant amino acceptor substrate for AGTs, including hAGT, AeAGT, AeHKT, and DrAGT (6, 7, 31). Detoxifying glyoxylic acid is the major function of AGTs in mammals, including human beings. It has been proposed that peroxisomal AGT is responsible for detoxifying glycolate-derived glyoxylic acid, whereas mitochondrial AGT plays a major role in detoxifying hydroxyproline-derived glyoxylic acid (32–37). In plants, AGT has been known to be involved in the photorespiratory glyoxylic acid cycle within peroxisomes (38, 39). In yeast, disruption of AGT can lead to glycine auxotrophy (40). The importance of hepatic AGT in minimizing endogenous oxalate production in some mammals has been clearly shown by the autosomal recessive disorder of glyoxylic acid metabolism primary hyperoxaluria type 1, a potentially lethal condition in which AGT deficiency leads to excessive oxalate synthesis and excretion and the deposition of insoluble calcium oxalate in the kidney (41, 42). Because there have not been any reports regarding the three-dimensional crystal structure of an AGT-glyoxylic acid complex, the structure reported here provides the essential basis for understanding the generic interaction of glyoxylic acid with AGTs. Structurally, glyoxylic acid lies near the internal aldimine, and the C-2 atom of glyoxylic acid is above the PLP C4A reactive center at a distance of 3.0 Å. As in the alanine complex, the carboxylate group of glyoxylic acid forms a tight ion pair with Arg^{356A} at a distance of 2.9 Å, and Ser^{155A} and Gly^{345A} backbone oxygen

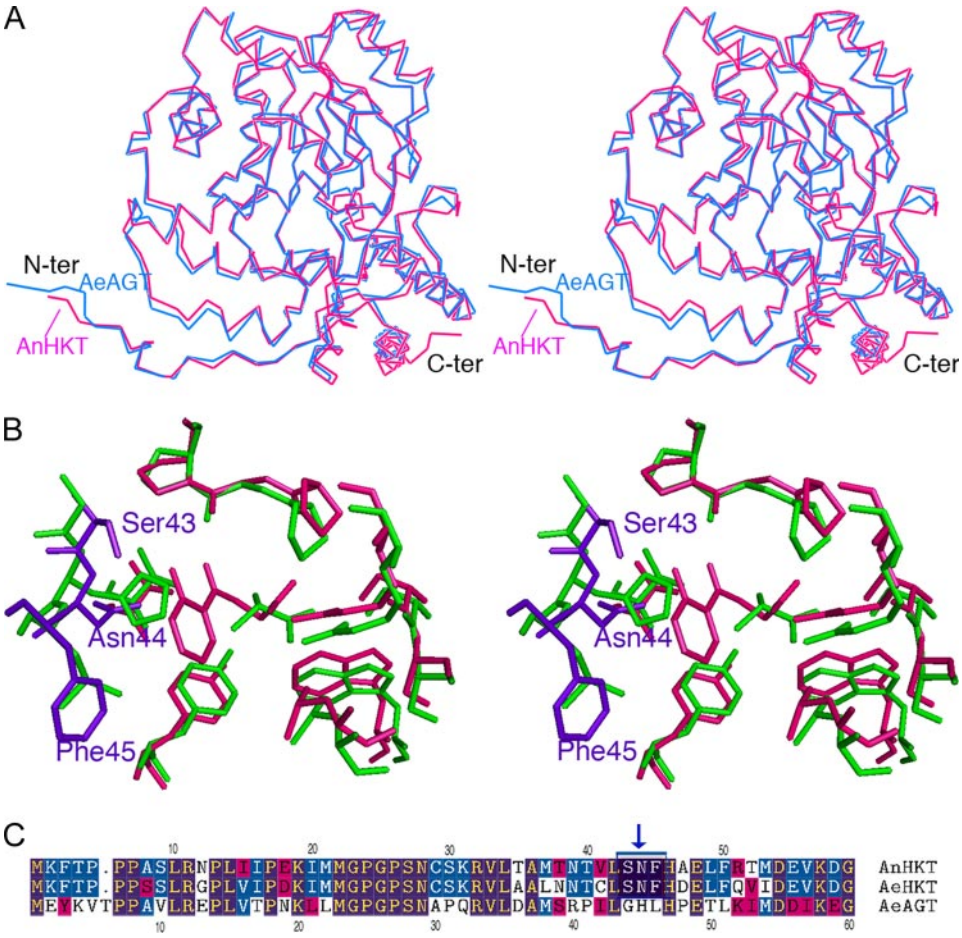

FIGURE 5. *A*, α-carbon representation in stereo of AeAGT (*blue*) superimposed onto AnHKT (*pink*). *B*, superposition of the AeAGT-alanine structure onto AnHKT-inhibitor structure. Only protein residues within 4 Å of alanine or AnHKT inhibitor are depicted as *sticks*. The residues and ligand from AeAGT are shown in *green*, and those from AnHKT are in *pink*. The residues in the AnHKT structure most likely involved in 3-HK recognition are labeled and are shown in *blue*. *C*, sequence alignment of AnHKT, AeHKT, and AeAGT. *Boxed sequences* (SNF) of two HKT enzymes are proposed for 3-HK recognition.

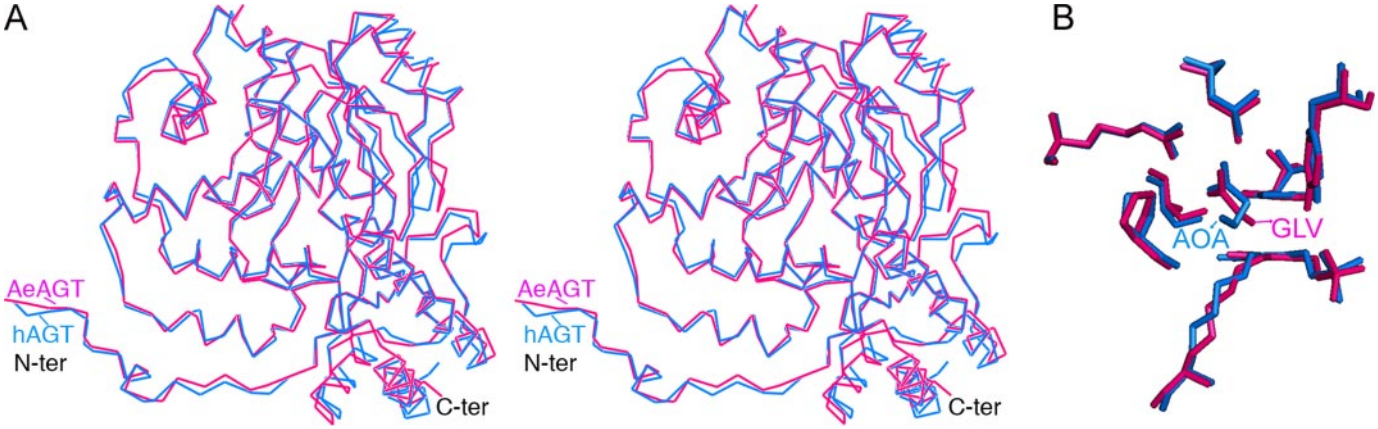

FIGURE 6. *A*, α-carbon representation in stereo of AeAGT (*pink*) superimposed onto hAGT (*blue*). *B*, superposition of the AeAGT-glyoxylic acid structure onto hAGT-amino-oxyacetic acid structure. Only protein residues within 4 Å of glyoxylic acid or amino-oxyacetic acid are depicted in *stick* form. The residues and glyoxylic acid (*GLV*) from AeAGT are colored in *red*, and residues and amino-oxyacetic acid (*AOA*) from hAGT are in *blue*.

atoms fix the Arg^{356A} side chain in the optimal conformation for glyoxylic acid binding. One oxygen atom of the glycine carboxylate group also forms a hydrogen bond with the side chain of Ser^{155A}. Other residues around the glyoxylic acid molecule within 4 Å are Tyr^{57B}, His^{45B}, Arg^{25A}, Ser^{155A}, LLPA, and Thr^{260B}, and in particular Tyr^{257B}, Pro^{25A}, and LLPA, which establish hydrophobic interactions with glyoxylic acid. Finally, Ser^{155A} OG is bound to the O-2 atom of glyoxylic acid (Fig. 4*B*).

Comparison with Other AGT Structures with Regard to Substrate Specificity—In principle, differences in enzyme function should be reflected in both the primary and three-dimensional structures. Based on the available three-dimensional crystal structures of AGTs, hAGT (17), yeast AGT (28), *Nostoc* AGT (29), AnHKT (14), and the one reported herein, all residues involved in PLP binding are conserved within the five structures (not shown). AnHKT shares 73% amino acid sequence identity with AeHKT, and an AnHKT-inhibitor complex structure with an inhibitor that is structurally similar to 3-HK and kynurenine has been determined (14). Both AnHKT and AeHKT exhibit high activity toward 3-HK and kynurenine (3, 7, 43), whereas AeAGT displays no activity toward 3-HK and kynurenine (6). On superposing the AeAGT-alanine complex onto the AnHKT-inhibitor structure (Fig. 5*A*), we identified the residues within 4 Å of both ligands and found that most residues are conserved. An exception was the Ser^{43}-Asn^{44}-Phe^{45} triad of AnHKT that is changed to Gly^{44A}-His^{45A}-Leu^{46A} in AeAGT (Fig. 5*B*). The amino acid sequence alignment shows that AeHKT and AnHKT share the same sequence in this area (*boxed* in Fig. 5*C*). The results suggest that the Ser-Asn-Phe motif is involved in 3-HK and kynurenine substrate recognition for mosquito HKTs. A future mutation experiment may confirm this hypothesis. Glyoxylic acid is the most suitable substrate for all AGTs, and therefore its binding site should be conserved in AGTs. A three-dimensional crystal structure of hAGT-amino-oxyacetic acid (AGT inhibitor) is available for comparison (17). On superposing hAGT structure onto the AeAGT-glyoxylic acid complex structure (Fig. 6*A*), we identified the residues within 4 Å of both ligands and found that all the residues (Ser, Pro, Arg, PLP, and Tyr (in the other unit)) were the same in both structures (Fig. 6*B*). The sequence comparison showed that *Anopheles* AGT, AeHKT, and AnHKT also shared the same residues for glyoxylic acid binding and that yeast AGT and *Nostoc* AGT shared similar residues, with Ser substituted by Thr.

In summary, evolution has led to the development of two AGTs, AGT and HKT, in the mosquito. This duplication occurred before the mosquito/fruit fly divergence. The primary function of the mosquito AGT and HKT enzymes is quite different. The three-dimensional structures of AeAGT and its complexes with alanine and glyoxylic acid obtained in this study, in comparison with the three-dimensional structure of the AnHKT, provide some reasonable explanation regarding the structural basis underlying the substrate specificity between mosquito AGT and HKT. As this is the first report of the structures of an AGT with its native substrates, it may also help in understanding the catalyzing mechanism of AGTs, particularly hAGT, which is related to a lethal condition in humans.

Acknowledgments—This work was carried out in part at the National Synchrotron Light Source, Brookhaven National Laboratory. The authors acknowledge the support of the Virginia Tech Department of Biological Sciences for the use of the X-ray facility.

REFERENCES

1. Snow, R. W., Guerra, C. A., Noor, A. M., Myint, H. Y., and Hay, S. I. (2005) *Nature* **434,** 214–217
2. Li, J., and Li, G. (1997) *Insect Biochem. Mol. Biol.* **27,** 859–867
3. Han, Q., Fang, J., and Li, J. (2002) *J. Biol. Chem.* **277,** 15781–15787
4. Garcia, G. E., Wirtz, R. A., Barr, J. R., Woolfitt, A., and Rosenberg, R. (1998) *J. Biol. Chem.* **273,** 12003–12005
5. Billker, O., Lindo, V., Panico, M., Etienne, A. E., Paxton, T., Dell, A., Rogers, M., Sinden, R. E., and Morris, H. R. (1998) *Nature* **392,** 289–292
6. Han, Q., Kim, S. R., Ding, H., and Li, J. (2006) *Biochem. J.* **397,** 473–481
7. Han, Q., and Li, J. (2002) *FEBS Lett.* **527,** 199–204
8. Guidetti, P., Okuno, E., and Schwarcz, R. (1997) *J. Neurosci. Res.* **50,** 457–465
9. Okuno, E., Nakamura, M., and Schwarcz, R. (1991) *Brain Res.* **542,** 307–312
10. Han, Q., and Li, J. (2004) *FEBS Lett.* **577,** 381–385
11. Han, Q., Gao, Y. G., Robinson, H., Ding, H., Wilson, S., and Li, J. (2005) *FEBS J.* **272,** 2198–2206
12. Fang, J., Han, Q., and Li, J. (2002) *Insect Biochem. Mol. Biol.* **32,** 943–950
13. Li, J., Beerntsen, B. T., and James, A. A. (1999) *Insect Biochem. Mol. Biol.* **29,** 329–338
14. Rossi, F., Garavaglia, S., Giovenzana, G. B., Arca, B., Li, J., and Rizzi, M. (2006) *Proc. Natl. Acad. Sci. U. S. A.* **103,** 5711–5716
15. Otwinowski, Z. (1993) in *Proceedings of CCP4 Study Weekend. Data Collection and Processing* (Sawyer, L., Isaacs, N., and Bailey, S., eds) pp. 80–86, Daresbury Laboratory, Warrington, UK
16. Minor, W. (1993) *XDISPLAYF Program*, Purdue University, West Lafayette, IN
17. Zhang, X., Roe, S. M., Hou, Y., Bartlam, M., Rao, Z., Pearl, L. H., and Danpure, C. J. (2003) *J. Mol. Biol.* **331,** 643–652
18. Vagin, A., and Teplyakov, A. (1997) *J. Appl. Crystallogr.* **30,** 1022–1025
19. Murshudov, G. N., Vagin, A. A., and Dodson, E. J. (1997) *Acta Crystallogr. Sect. D Biol. Crystallogr.* **53,** 240–255
20. Jones, T. A., Zou, J. Y., Cowan, S. W., and Kjeldgaard, M. (1991) *Acta Crystallogr. Sect. A.* **47**, 110–119
21. Perrakis, A., Sixma, T. K., Wilson, K. S., and Lamzin, V. S. (1997) *Acta Crystallogr. Sect. D Biol. Crystallogr.* **53,** 448–455
22. Kabsch, W. (1976) *Acta Crystallogr. Sect. A* **32**, 922–923
23. Wallace, A. C., Laskowski, R. A., and Thornton, J. M. (1995) *Protein Eng.* **8,** 127–134
24. DeLano, W. L. (2002) *The PyMOL Molecular Graphics System*, DeLano Scientific, San Carlos, CA
25. Laskowski, R. A., Macarthur, M. W., Moss, D. S., and Thornton, J. M. (1993) *J. Appl. Crystallogr.* **26,** 283–291
26. Jansonius, J. N. (1998) *Curr. Opin. Struct. Biol.* **8,** 759–769
27. Nakai, T., Okada, K., Akutsu, S., Miyahara, I., Kawaguchi, S., Kato, R., Kuramitsu, S., and Hirotsu, K. (1999) *Biochemistry* **38,** 2413–2424
28. Meyer, P., Liger, D., Leulliot, N., Quevillon-Cheruel, S., Zhou, C. Z., Borel, F., Ferrer, J. L., Poupon, A., Janin, J., and van Tilbeurgh, H. (2005) *Biochimie* (*Paris*) **87,** 1041–1047
29. Han, G. W., Schwarzenbacher, R., Page, R., Jaroszewski, L., Abdubek, P., Ambing, E., Biorac, T., Canaves, J. M., Chiu, H. J., Dai, X., Deacon, A. M., DiDonato, M., Elsliger, M. A., Godzik, A., Grittini, C., Grzechnik, S. K., Hale, J., Hampton, E., Haugen, J., Hornsby, M., Klock, H. E., Koesema, E., Kreusch, A., Kuhn, P., Lesley, S. A., Levin, I., McMullan, D., McPhillips, T. M., Miller, M. D., Morse, A., Moy, K., Nigoghossian, E., Ouyang, J., Paulsen, J., Quijano, K., Reyes, R., Sims, E., Spraggon, G., Stevens, R. C., van den Bedem, H., Velasquez, J., Vincent, J., von Delft, F., Wang, X., West, B., White, A., Wolf, G., Xu, Q., Zagnitko, O., Hodgson, K. O., Wooley, J., and Wilson, I. A. (2005) *Proteins* **58,** 971–975

30. Okamoto, A., Nakai, Y., Hayashi, H., Hirotsu, K., and Kagamiyama, H. (1998) *J. Mol. Biol.* **280,** 443–461
31. Okuno, E., Minatogawa, Y., Nakamura, M., Kamoda, N., Nakanishi, J., Makino, M., and Kido, R. (1980) *Biochem. J.* **189,** 581–590
32. Birdsey, G. M., Lewin, J., Holbrook, J. D., Simpson, V. R., Cunningham, A. A., and Danpure, C. J. (2005) *Proc. Biol. Sci.* **272,** 833–840
33. Birdsey, G. M., Lewin, J., Cunningham, A. A., Bruford, M. W., and Danpure, C. J. (2004) *Mol. Biol. Evol.* **21,** 632–646
34. Takayama, T., Fujita, K., Suzuki, K., Sakaguchi, M., Fujie, M., Nagai, E., Watanabe, S., Ichiyama, A., and Ogawa, Y. (2003) *J. Am. Soc. Nephrol.* **14,** 939–946
35. Holbrook, J. D., and Danpure, C. J. (2002) *J. Biol. Chem.* **277,** 2336–2344
36. Danpure, C. J. (1997) *BioEssays* **19,** 317–326
37. Watts, R. W. (1992) *Adv. Enzyme Regul.* **32,** 309–327
38. Rehfeld, D. W., and Tolbert, N. E. (1972) *J. Biol. Chem.* **247,** 4803–4811
39. Liepman, A. H., and Olsen, L. J. (2001) *Plant J.* **25,** 487–498
40. Schlosser, T., Gatgens, C., Weber, U., and Stahmann, K. P. (2004) *Yeast* **21,** 63–73
41. Danpure, C. J. (2001) in *The Molecular and Metabolic Bases of Inherited Disease* (Scriver, C. R., Beaudet, A. L., Sly, W. S., Valle, D., Childs, B., Kinzler, K. W., and Vogelstein, B., eds) pp. 3323–3367, McGraw-Hill, New York
42. Danpure, C. J., Jennings, P. R., Leiper, J. M., Lumb, M. J., and Oatey, P. B. (1996) *Ann. N. Y. Acad. Sci.* **804,** 477–490
43. Rossi, F., Lombardo, F., Paglino, A., Cassani, C., Miglio, G., Arca, B., and Rizzi, M. (2005) *FEBS J.* **272,** 5653–5662

Crystal Structures of *Aedes aegypti* Alanine Glyoxylate Aminotransferase

Qian Han, Howard Robinson, Yi Gui Gao, Nancy Vogelaar, Scott R. Wilson, Menico Rizzi and Jianyong Li

J. Biol. Chem. 2006, 281:37175-37182.
doi: 10.1074/jbc.M607032200 originally published online September 21, 2006
